Shape evolution and coexistence in neutron-deficient Nd and Sm nuclei

J. Xiang,[1] Z. P. Li,[2,1,*] W. H. Long,[3] T. Nikšić,[4] and D. Vretenar[4]

[1]*School of Physics and Electronic, Qiannan Normal University for Nationalities, Duyun 558000, China*
[2]*School of Physical Science and Technology, Southwest University, Chongqing 400715, China*
[3]*School of Nuclear Science and Technology, Lanzhou University, Lanzhou 730000, China*
[4]*Physics Department, Faculty of Science, University of Zagreb, Croatia*

The evolution of shapes and low-energy shape coexistence is analyzed in neutron-deficient Nd and Sm nuclei, using a five-dimensional quadrupole collective Hamiltonian (5DCH). Deformation energy surfaces, calculated with the relativistic energy density functional PC-PK1 and a separable finite-range pairing interaction, exhibit a transition from spherical shapes near $N = 80$, to γ-soft shapes, and to prolate deformed minima in lighter isotopes. The corresponding 5DCH model calculation, based on the self-consistent mean-field potentials, reproduces the empirical isotopic trend of characteristic collective observables, and predicts significantly different deformations for the first two 0^+ states in the $N = 74$ isotones ^{134}Nd and ^{136}Sm. In addition to bands based on the triaxial γ-soft ground state, in excellent agreement with data, the occurrence of a low-energy rotational band is predicted, built on the prolate deformed ($\beta \sim 0.4$) excited state 0_2^+.

I. INTRODUCTION

An interesting phenomenon that occurs in many mesoscopic systems is shape coexistence: sets of nearly degenerate low-energy states are observed that can be characterized by different geometrical shapes. In atomic nuclei, in particular, coexistence of different shapes in a single nucleus, and shape transitions as a function of nucleon number, have been observed in light, medium-heavy, and heavy systems [1–3]. The distinctive character of shape coexistence in nuclei reflects the interplay between single-particle and collective degrees of freedom. Experimental and theoretical studies of shapes, their evolution and transitions, provide crucial information on the origin of nuclear collectivity and modification of shell structures in nuclei far from stability [4]. In a recent systematic analysis of characteristic signatures of coexisting nuclear shapes in different mass regions [5], quadrupole shape invariants for more than 600 even-even nuclei were calculated using a global self-consistent theoretical method based on universal energy density functionals (EDFs) and the quadrupole collective model. A systematic comparison of shape invariants for the two lowest 0^+ states has identified regions of possible shape coexistence. Different geometric shapes at low energies emerge as a universal structure property that occurs in different mass regions over the entire chart of nuclides.

Neutron-deficient rare-earth nuclei in the mass $A \approx 140$ region are known to exhibit a variety of coexisting structures resulting from the midshell filling of the $h_{11/2}$ intruder orbital. Protons fill the lower part of the $h_{11/2}$ shell with low-Ω

orbitals favoring a prolate nuclear deformation, whereas for neutrons the Fermi surface lies close to high-Ω $h_{11/2}$ states, favoring oblate shapes. This competition between opposing trends for proton and neutron deformations can produce γ-soft ground-state shapes with a significant degree of triaxiality. Calculations by Möller and Bengtsson [6], based on the finite-range droplet model, predicted the ground states of neutron-deficient $A \sim 140$ nuclei to be triaxial. In addition, several studies indicated that the γ degree of freedom plays an important role in the description of collective excited states [7–11]. These nuclei exhibit additional interesting structure effects, with the observation of isomeric states [7,12,13], and magnetic rotation [14,15]. Based on experimental results, it has been suggested that ^{144}Dy [16] and ^{142}Sm [17] exhibit possible shape coexistence. Furthermore, in Ref. [5], medium-deformed triaxial ground states coexisting with highly deformed prolate excited state have been predicted in this region, especially for the nuclei ^{134}Nd, ^{136,138}Sm, ^{140,142}Gd, and ^{142,144}Dy.

Rare-earth nuclei with neutron number $N \approx 90$ present some of the best examples of shape phase transitions. Employing a consistent framework of structure models based on energy density functionals, in several studies we analysed microscopic signatures of ground-state shape phase transitions in this region of the nuclear mass table. In the present work we consider shape evolution and the possible occurrence of shape coexistence in neutron-deficient Nd and Sm isotopes. The analysis starts from self-consistent mean-field calculations of deformation energy surfaces using relativistic energy density functionals [18–21], and is extended to include the treatment of collective correlations with the five-dimensional collective Hamiltonian (5DCH) model. This approach has successfully been applied to the description of low-lying collective states

---

*zpliphy@swu.edu.cn

in a wide range of nuclei, from the mass region $A \sim 40$ to superheavy systems [22–34].

In Sec. II we present a short outline of the theoretical framework used to study shape coexistence in neutron-deficient $A \sim 140$ nuclei. The systematics of collective deformation energy surfaces, the evolution of characteristic signatures of deformed shapes, and the low-energy spectra of ^{134}Nd and ^{136}Sm are discussed in Sec. III. Section IV summarizes the principal results.

II. THE 5D COLLECTIVE HAMILTONIAN

Nuclear EDF-based studies of low-energy structure phenomena start from a self-consistent mean-field (SCMF) calculation of deformation energy surfaces with mass multipole moments as constrained quantities. The results are static symmetry-breaking product many-body states. The static nuclear mean-field is characterized by the breaking of symmetries of the underlying Hamiltonian—translational, rotational, particle number, and, therefore, includes static correlations, e.g., deformations and pairing. To calculate excitation spectra and electromagnetic transition rates it is necessary to extend the SCMF scheme to include collective correlations that arise from symmetry restoration and fluctuations around the mean-field minima.

Low-energy excitation spectra and transitions can be described using a collective Hamiltonian, with deformation-dependent parameters determined from microscopic SCMF calculations. For instance, in the case of quadrupole degrees of freedom, excitations determined by quadrupole vibrational and rotational degrees of freedom can be described by considering two quadrupole collective coordinates β, γ and three Euler angles $\Omega \equiv (\phi, \theta, \psi)$ [22]. The corresponding 5DCH Hamiltonian takes the following form:

$$\hat{H}(\beta, \gamma, \Omega) = \hat{T}_{\text{vib}} + \hat{T}_{\text{rot}} + V_{\text{coll}}, \quad (1)$$

where V_{coll} is the collective potential that includes zero-point energy (ZPE) corrections, and $\hat{T}_{\text{vib}}$ and $\hat{T}_{\text{rot}}$ are the vibrational and rotational kinetic energy terms, respectively [22,35,36],

$$\hat{T}_{\text{vib}} = -\frac{\hbar^2}{2\sqrt{wr}} \left\{ \frac{1}{\beta^4} \left[\frac{\partial}{\partial \beta} \sqrt{\frac{r}{w}} \beta^4 B_{\gamma\gamma} \frac{\partial}{\partial \beta} - \frac{\partial}{\partial \beta} \sqrt{\frac{r}{w}} \beta^3 B_{\beta\gamma} \frac{\partial}{\partial \gamma} \right] \right.$$
$$+ \frac{1}{\beta \sin 3\gamma} \left[-\frac{\partial}{\partial \gamma} \sqrt{\frac{r}{w}} \sin 3\gamma B_{\beta\gamma} \frac{\partial}{\partial \beta} \right.$$
$$+ \left. \left. \frac{1}{\beta} \frac{\partial}{\partial \gamma} \sqrt{\frac{r}{w}} \sin 3\gamma B_{\beta\beta} \frac{\partial}{\partial \gamma} \right] \right\}, \quad (2)$$

$$\hat{T}_{\text{rot}} = \frac{1}{2} \sum_{k=1}^{3} \frac{\hat{J}_k^2}{\mathcal{I}_k}. \quad (3)$$

$\hat{J}_k$ denotes the components of the angular momentum in the body-fixed frame of a nucleus, and $B_{\beta\beta}$, $B_{\beta\gamma}$, $B_{\gamma\gamma}$, are the mass parameters. Two additional quantities that appear in $\hat{T}_{\text{vib}}$, namely, $r = B_1 B_2 B_3$ (see Ref. [22] for the definition of B_k), and $w = B_{\beta\beta} B_{\gamma\gamma} - B_{\beta\gamma}^2$, determine the volume element in the collective space. The constrained SCMF solutions for the single-quasiparticle energies and wave functions for the entire energy surface, as functions of the quadrupole deformations

β and γ, provide the microscopic input for calculation of the mass parameters, moments of inertia, and the collective potential. The Hamiltonian describes quadrupole vibrations, rotations, and the coupling of these collective modes. The dynamics of the 5DCH is governed by the seven functions of the intrinsic deformations β and γ: the collective potential $V_{\text{coll}}(\beta, \gamma)$, three mass parameters $B_{\beta\beta}(\beta, \gamma)$, $B_{\beta\gamma}(\beta, \gamma)$, and $B_{\gamma\gamma}(\beta, \gamma)$, and three moments of inertia $\mathcal{I}_k(\beta, \gamma)$ ($k = 1, 2, 3$). The corresponding eigenvalue equation is solved by expanding the eigenfunctions on a complete set of basis functions that depend on the deformation variables β and γ, and the Euler angles [35].

III. NEUTRON-DEFICIENT ND AND SM ISOTOPES

Just as our recent global analysis of quadrupole shape invariants [5], the present study starts from a quadrupole deformation-constrained relativistic mean-field (RMF) plus Bardeen-Cooper-Schrieffer (BCS) pairing correlation calculation, with the point-coupling energy functional PC-PK1 [37] and a separable pairing interaction [38] in the particle-hole and particle-particle channels, respectively. The SCMF single-nucleon Dirac equation is solved by expanding the Dirac spinor in terms of a three-dimensional (3D) harmonic oscillator basis with 14 major shells. The SCMF states are calculated on the grid: $\beta \in [0.0, 0.8]$ and $\gamma \in [0°, 60°]$ with $\Delta\beta = 0.05$ and $\Delta\gamma = 6°$. More details about the mean-field calculations can be found in Refs. [39,40]. For the collective Hamiltonian (1) the mass parameters and moments of inertia are determined in the perturbative cranking approximation using the SCMF triaxial quasiparticle states [22]. Diagonalization of the 5DCH generates the excitation spectra and collective wave functions that are used to calculate spectroscopic properties, such as electric multipole transition strengths [22].

Figure 1 displays the collective potential energy surface in the β-γ plane for even-even neutron-deficient isotopes $^{126-140}$Nd. For each nucleus the calculated energies are normalized with respect to the binding energy of the absolute minimum. The corresponding deformation energy maps of the even-even isotopes $^{128-142}$Sm are shown in Fig. 2. For both isotopic chains these plots illustrate a rapid transition from spherical shapes near $N = 80$, to γ-soft shapes, and then to prolate deformed energy surfaces in lighter isotopes. Starting from the spherical nuclei ^{140}Nd and ^{142}Sm, a certain degree of triaxiality develops in ^{138}Nd and ^{140}Sm, followed by the occurrence of γ-soft minima in ^{136}Nd and ^{138}Sm. At neutron number $N = 74$, both Nd and Sm exhibit a coexistence of γ-soft and axially deformed prolate shapes. For $N \leqslant 72$ isotopes only well-deformed axially symmetric prolate minima are predicted by the SCMF calculation.

In Figs. 3 and 4 we analyze the evolution of several quantities that can be used to characterize transitions between different shapes as functions of the neutron number: the energy ratio $R_{42} = \frac{E(4^+) - E(0^+)}{E(2^+) - E(0^+)}$ and the $B(E2; 2^+ \to 0^+)$ values for the ground-state band and the band based on 0_2^+, the energy ratio $E(2_\gamma^+)/E(4_1^+)$, the excitation energy of the 0_2^+ state, and the quadrupole deformation parameters β and γ in the ground state 0_1^+ and the first excited 0_2^+. For the even-even Nd and
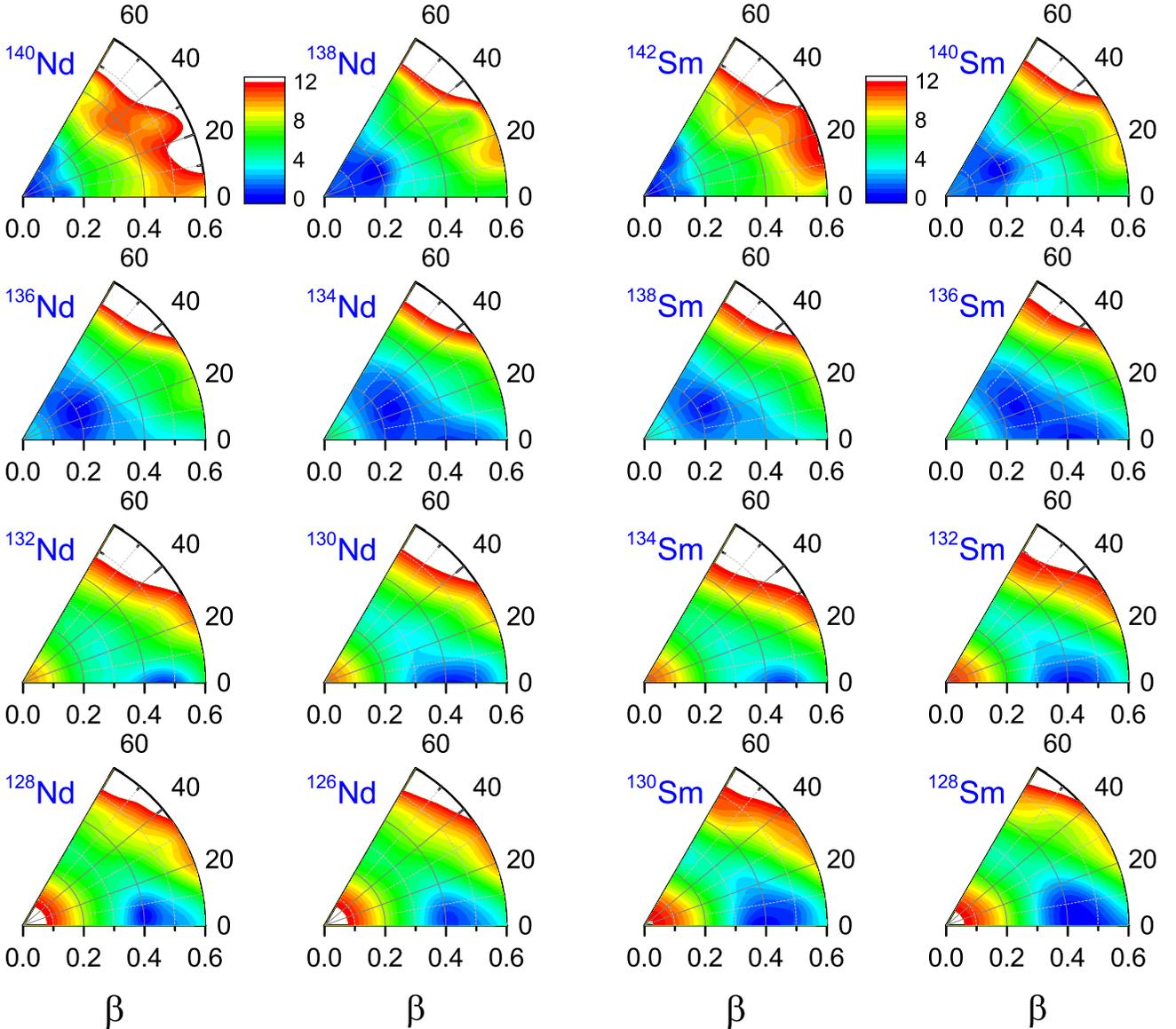
FIG. 1. Collective potential energy V_{coll} of the even-even isotopes $^{126-140}$Nd in the (β, γ) plane, obtained by constrained relativistic mean-field plus BCS calculations. For each nucleus energies are normalized to the absolute minimum. The energy difference between neighboring contours is 0.5 MeV.

FIG. 2. Same as in the caption to Fig. 1 but for the neutron-deficient isotopes of Sm.

Sm isotopes these quantities are calculated using the 5DCH, with parameters determined by the SCMF solutions shown in Figs. 1 and 2. Where available, the results are shown in comparison to data [41]. The evolution of R_{42} characterizes shape transitions between axially deformed rotors ($R_{42} = 3.33$), γ-soft shapes ($R_{42} = 2.50$), and spherical vibrational nuclei ($R_{42} = 2.00$). One notices how the energy ratio R_{42} for the ground-state band decreases from the rotational value $R_{42} \sim 3.3$ at $N \sim 66$ to the transitional γ-soft value $R_{42} \sim 2.5$ in the region $N = 74$–78, in excellent agreement with the empirical trend. A similar behavior, with the significant exception of ^{136}Sm, is also predicted for the sequence of levels

built on the first excited 0^+ state. As shown in Figs. 3(c) and 4(c), the ratio $E(2_\gamma^+)/E(4_1^+)$ calculated with the 5DCH in Nd and Sm isotopes is in excellent agreement with the available data. The predicted values ~ 1.0 for this energy ratio at $N = 74$–78 characterize the occurrence of low-energy γ-deformed structures in these isotopes.

Figures 3(b) and 4(b) display the values $B(E2; 2^+ \rightarrow 0^+)$ for the transitions from the first state 2_1^+ to the ground state, and for the state 2^+ built on the excited 0_2^+ state, in the Nd and Sm isotopes, respectively. The corresponding experimental values $B(E2; 2_1^+ \rightarrow 0_1^+)$ [41] are shown for comparison. The 5DCH calculation reproduce the data, and one notices the gap between the value $B(E2)$ for the ground-state sequence and the corresponding value for the state built on the 0_2^+ state, in ^{134}Nd and ^{136,138}Sm. This indicates that in these isotopes the
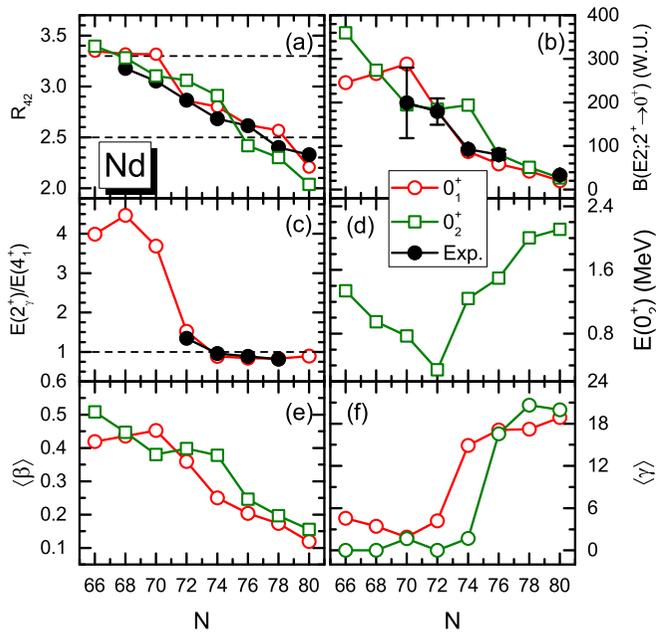
FIG. 3. The energy ratio $R_{42} = \frac{E(4^+) - E(0^+)}{E(2^+) - E(0^+)}$ (a) and $B(E2; 2^+ \rightarrow 0^+)$ values (b) for the ground-state band and the band based on the 0_2^+ state, the energy ratio $E(2_\gamma^+)/E(4_1^+)$ (c), the excitation energy of the 0_2^+ state $E(0_2^+)$ (d), the values of the quadrupole deformation parameters β (e), and γ (f) for the 0_1^+ and 0_2^+ state, as functions of the neutron number in Nd isotopes. The data are from Ref. [41].

average deformations $\langle \beta \rangle$ for the ground state 0_1^+ differ from those of the 0_2^+ state, as also shown in Figs. 3(e) and 4(e). The energies of the first excited 0^+ state of Nd and Sm isotopes are shown in Figs. 3(d) and 4(d), respectively. For both chains $E(0_2^+)$ decreases from $N = 66$ to $N = 72$, where it displays a
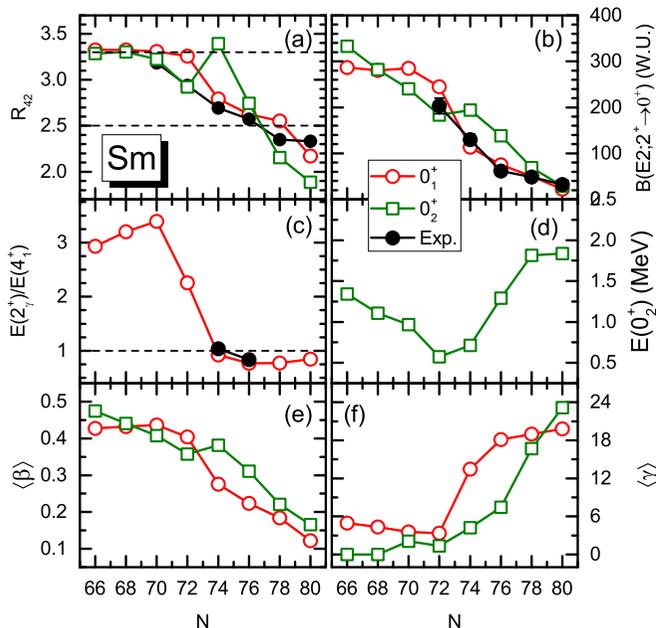

FIG. 4. Same as in the caption to Fig. 3 but for the chain of Sm isotopes.
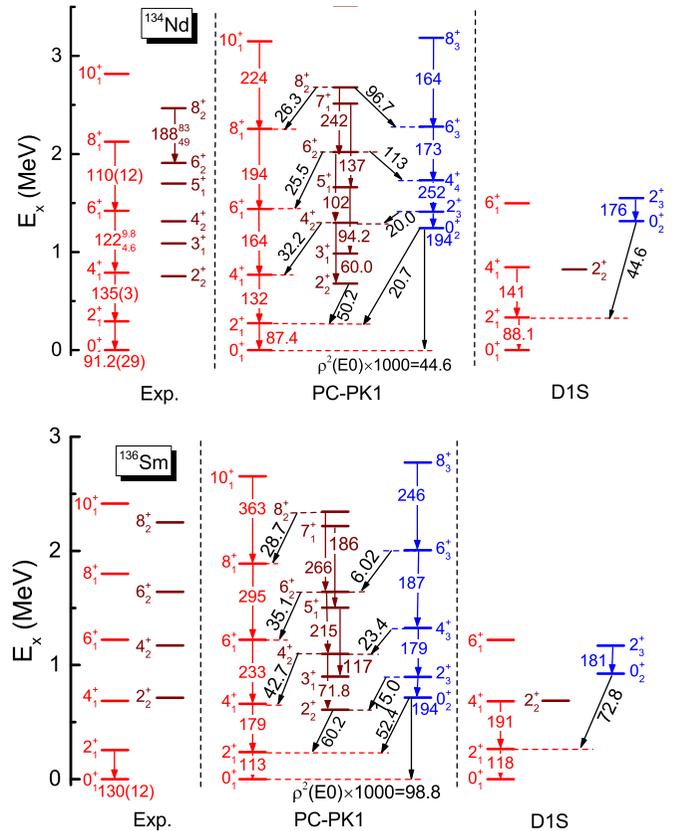

FIG. 5. 5DCH energy spectra of ^{134}Nd and ^{136}Sm (PC-PK1), compared to available data [41,42] (Exp.), and to results obtained with the 5DCH based on the Gogny force (D1S) [43].

pronounced minimum, and then increases sharply toward the neutron closed shell at $N = 82$. This behavior clearly reflects the evolution of the collective potential energy surfaces from prolate deformed to γ soft, and to spherical shapes, as shown in Figs. 1 and 2.

The occurrence of shape coexistence can be further illustrated by analyzing the evolution of average quadrupole deformations $\langle \beta \rangle$ and $\langle \gamma \rangle$ for the two lowest 0^+ states. In Figs. 3 and 4 we plot the deformations $\langle \beta \rangle$ and $\langle \gamma \rangle$ for 0_1^+ and 0_2^+, as functions of neutron number in Nd and Sm isotopes, respectively. The average deformations are determined from the calculated quadrupole shape invariants following the procedure described in Ref. [5]. Note that, while they exhibit similar trends, marked differences between 0_1^+ and 0_2^+ are predicted in several nuclei, especially at $N = 74$. In ^{134}Nd the values of $\langle \beta \rangle$ for the 0_1^+ and 0_2^+ states are ~ 0.25 and ~ 0.4, and the corresponding $\langle \gamma \rangle$ are $\sim 15°$ and $2°$, respectively. Therefore, not only the SCMF potential energy surface, but also the 5DCH model calculation predicts a coexistence of soft triaxial and prolate axially deformed low-energy structures in ^{134}Nd. A very similar picture is also found in ^{136}Sm.

For these two nuclei in Fig. 5 we display the 5DCH low-energy spectra obtained in the present study (PC-PK1) and with the Gogny force (D1S) [43], in comparison with available data [41,42]. Both models, without any additional adjustment, reproduce the excitation energies and $E2$-transition

rates of the two lowest bands based on the γ-soft ground state. In particular, we note that the very low band-head 2_γ^+ of the γ band is calculated slightly below 4_1^+ in ^{134}Nd, in excellent agreement with experiment. Both 5DCH calculations predict the occurrence of a rotational sequence of levels in ^{134}Nd and ^{136}Sm, based on the low-lying 0_2^+ state, that is, structures built on the prolate deformed minima shown in Figs. 1 and 2. Compared to the yrast sequences, these bands are characterized by larger moments of inertia and enhanced $E2$-transition rates for the few lowest levels. For higher angular momenta one expects considerable mixing between the two structures. The calculated $E0$-transition strengths $\rho^2(E0; 0_2^+ \to 0_1^+) \times 10^3$ are 44.6 for ^{134}Nd, and 98.8 for ^{136}Sm, comparable to the values that characterize the well-known shape-coexisting nuclei ^{98}Sr [51(5)] and ^{100}Zr [108(19)] [44]. The bands built on the 0_2^+ states have not yet been observed and it would, therefore, be very important to be able to experimentally confirm the predicted shape coexistence in these $N = 74$ isotones.

Shape coexistence in the 5DCH model is best illustrated by considering the probability density distributions that correspond to the collective wave functions in the β-γ plane. The eigenfunctions of the collective Hamiltonian read

$$\Psi_\alpha^{JM}(\beta, \gamma, \Omega) = \sum_{K \in \Delta J} \psi_{\alpha K}^J(\beta, \gamma)\Phi_{MK}^J(\Omega). \quad (4)$$

For a given collective state, the probability distribution in the (β, γ) plane is defined as

$$\rho_{J\alpha}(\beta, \gamma) = \sum_{K \in \Delta J} \left|\psi_{\alpha K}^J(\beta, \gamma)\right|^2 \beta^3 \quad (5)$$

with the summation over the allowed set of values of the projection K of the angular momentum J on the body-fixed symmetry axis, and with the normalization

$$\int_0^\infty \beta d\beta \int_0^{2\pi} \rho_{J\alpha}(\beta, \gamma)|\sin 3\gamma|d\gamma = 1. \quad (6)$$

Figure 6 displays the distribution of probability density $\rho_{J\alpha}(\beta, \gamma)$ in the β-γ plane for the two lowest levels of the yrast sequence and the prolate band based on 0_2^+, for ^{134}Nd and ^{136}Sm. These distributions clearly show that the two lowest collective states correspond to a triaxial but γ-soft geometric shape, whereas the collective wave functions of the states 0_2^+ and 2_3^+ are concentrated on the prolate axis at considerably larger axial deformation $\beta \sim 0.4$.

The rapid transition from triaxial-soft to prolate shape around $N \approx 74$ can be understood from a microscopic point of view by considering the evolution of neutron and proton single-particle levels as functions of deformation and particle number. Namely, the formation of deformed minima is related to the occurrence of regions of low single-particle level density around the Fermi surface. In Fig. 7 we plot the neutron (upper panel) and proton (lower panel) single-particle levels of ^{134}Nd, as functions of the deformation parameters along a closed path in the β-γ plane. Solid (black) curves correspond to levels with positive parity, and dashed (red) curves denote negative-parity levels. The dotted (blue) curves correspond to the Fermi levels. Starting from the spherical configuration, we follow the single-nucleon levels on a path
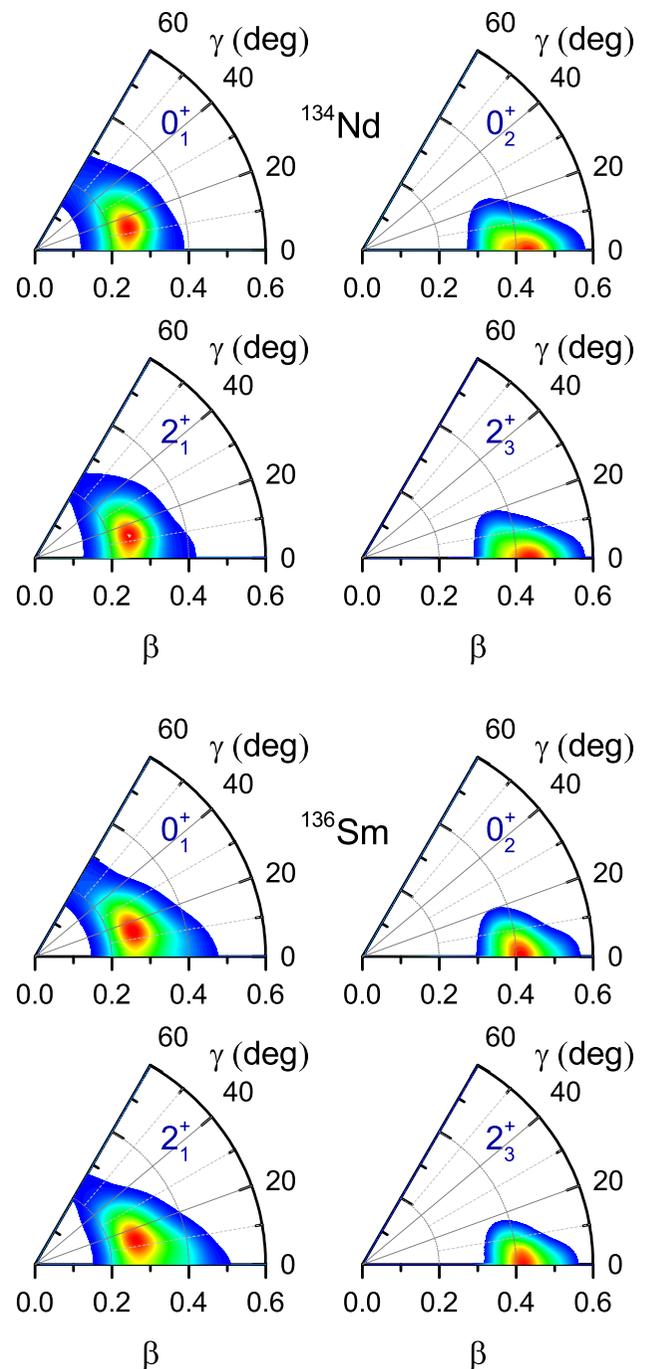

FIG. 6. Distribution of the probability density $\rho_{J\alpha}(\beta, \gamma)$ Eq. (5) for 0_1^+, 0_2^+, 2_1^+, and 2_3^+ collective states of ^{134}Nd and ^{136}Sm.

along the prolate axis up to the approximate position of the mean-field minimum (left panel), then for this fixed value of β the path from $\gamma = 0°$ to $\gamma = 60°$ (middle panel) and, finally, back to the spherical configuration along the oblate axis (right panel). Configurations along the oblate axis are denoted by negative values of β. One notices that both neutron and proton levels display pronounced gaps between the last occupied and first unoccupied states in the triaxial region close to $\gamma \sim 20°$ (neutrons) and $\gamma \sim 30°$ (protons). These gaps give
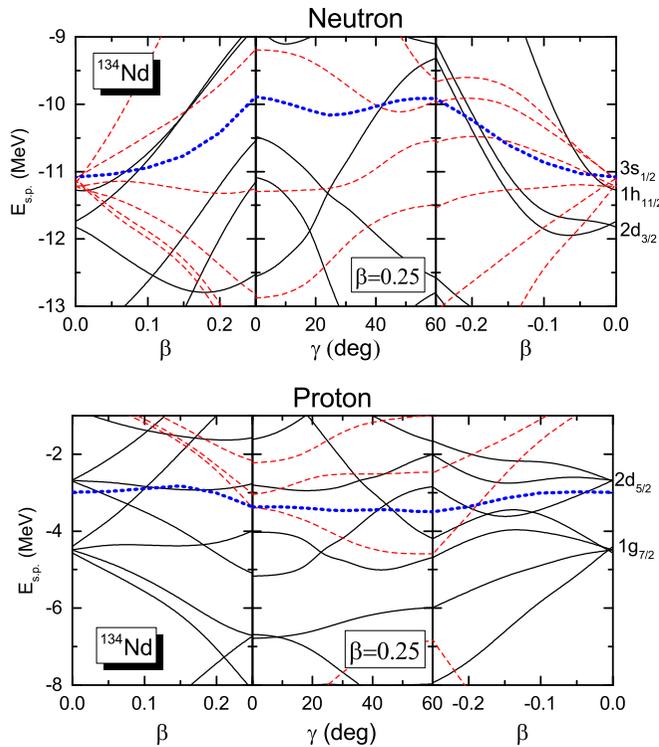
FIG. 7. Neutron (upper panel) and proton (lower panel) single-nucleon energy levels of ^{134}Nd, as functions of the deformation parameters along a closed path in the β-γ plane. Solid (black) curves correspond to levels with positive parity, and dashed (red) curves denote negative-parity levels. The dotted (blue) curves correspond to the Fermi levels. The panels on the left and right display prolate ($\gamma = 0°$) and oblate ($\gamma = 60°$) axially symmetric single-particle levels, respectively. In the middle panel the proton and neutron levels are plotted as functions of γ for a fixed value $|\beta| = 0.25$, corresponding to the approximate position of the mean-field minimum.

rise to the triaxial γ-soft minimum shown in Fig. 1 (cf. also the distribution of the probability density for the states 0_1^+ and 2_1^+ in Fig. 6). The origin of the low-lying prolate minimum in ^{134}Nd, on which the band based on 0_2^+ is built (cf. the states 0_2^+ and 2_3^+ in Fig. 6), can be found in the large energy gap for
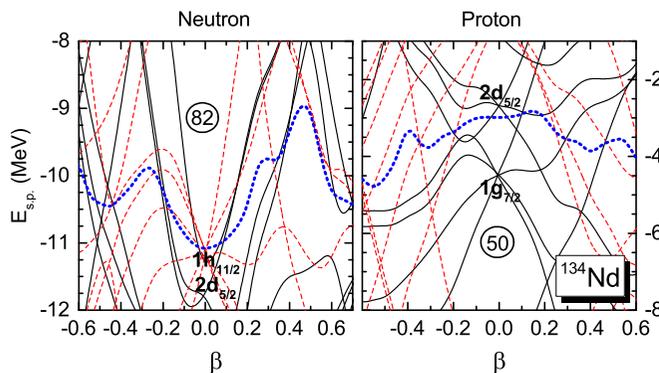

FIG. 8. Single-neutron and single-proton levels in ^{134}Nd as functions of the axial deformation parameter β. Solid (black) and dashed (red) curves denote the positive- and negative-parity levels, respectively. The dotted (blue) curves are the corresponding Fermi levels.
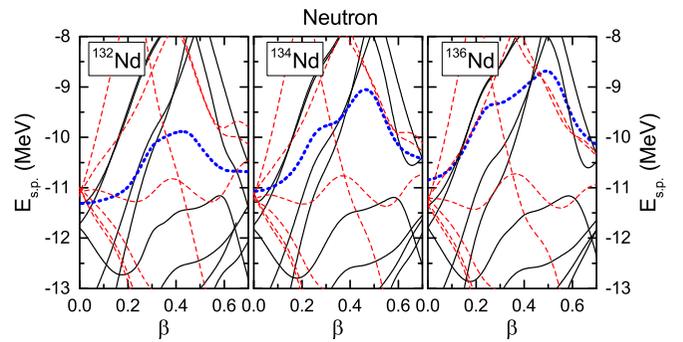

FIG. 9. Single-neutron levels in ^{132,134,136}Nd isotopes as functions of the axial deformation parameter β. Solid (black) and dashed (red) curves correspond to the positive- and negative-parity levels, respectively. The dotted (blue) curves denote the Fermi levels.

the proton levels at $\beta \approx 0.4$, as shown in Fig. 8. By decreasing the number of neutrons by two, one reaches ^{132}Nd. The proton levels do not change much, of course, whereas the neutron Fermi level is lowered in energy. As a result the pronounced triaxial gap present in the single-neutron spectrum of ^{134}Nd (cf. Fig. 7) disappears, while a large gap is formed among the axial single-neutron levels at $\beta \approx 0.5$. This is illustrated in Fig. 9, where we plot the single-neutron levels in ^{132,134,136}Nd as functions of the axial deformation parameter β. Together with the proton gap at $\beta \approx 0.4$, the large gap exhibited by the neutron levels leads to the formation of the prolate equilibrium minimum in ^{132}Nd, as shown in Fig. 1.

IV. SUMMARY

We have analyzed the evolution of shapes and possible occurrence of low-energy shape coexistence in neutron-deficient Nd and Sm nuclei. Fully self-consistent mean-field triaxial calculations, based on the relativistic energy density functional PC-PK1 and a separable finite-range pairing interaction, have been performed to produce deformation energy surfaces in the (β, γ) plane. These surfaces display a transition from spherical shapes near $N = 80$, to γ-soft shapes, and eventually to pronounced prolate deformed minima in lighter isotopes. In particular, the Nd and Sm $N = 74$ isotones exhibit coexisting low-energy γ-soft and axially deformed prolate minima.

The SCMF deformation-constrained solutions provide a microscopic input for the parameters of the 5D quadrupole collective Hamiltonian that has been used to calculate spectroscopic properties of low-energy states. The 5DCH model calculation reproduces the empirical isotopic trend of the characteristic collective observables $R_{42} = \frac{E(4^+) - E(0^+)}{E(2^+) - E(0^+)}$, $B(E2; 2^+ \rightarrow 0^+)$, and $E(2_\gamma^+)/E(4_1^+)$, while the values of $\langle \beta \rangle$, $\langle \gamma \rangle$ for the first two 0^+ states indicate significantly different deformations of these states in ^{134}Nd and ^{136}Sm. The theoretical low-energy collective spectra of these two nuclei, including excitation energies and $E2$ transition rates, are in excellent agreement with the available data. In addition to the bands based on the triaxial γ-soft ground state, the model predicts the occurrence of a low-energy rotational band built

on the prolate deformed ($\beta \sim 0.4$) excited state 0_2^+. ^{134}Nd and ^{136}Sm therefore present a very nice example of coexisting triaxial and prolate deformed shapes at low energy in neutron deficient rare-earth nuclei.

ACKNOWLEDGMENTS

[1] K. Heyde and J. L. Wood, Rev. Mod. Phys. **83**, 1467 (2011).

[2] K. Heyde, P. V. Isacker, M. Waroquier, J. L. Wood, and R. A. Meyer, Phys. Rep. **102**, 291 (1983).

[3] J. L. Wood, K. Heyde, W. Nazarewicz, M. Huyse, and P. V. Duppen, Phys. Rep. **215**, 101 (1992).

[4] K. Wrzosek-Lipska and L. P. Gaffney, J. Phys. G: Nucl. Part. Phys. **43**, 024012 (2016).

[5] S. Quan, Q. Chen, Z. P. Li, T. Nikšić, and D. Vretenar, Phys. Rev. C **95**, 054321 (2017).

[6] P. Möller, R. Bengtsson, B. G. Carlsson, P. Olivius, T. Ichikawa, H. Sagawa, and A. Iwamoto, At. Data Nucl. Data Tables **94**, 758 (2008).

[7] W. Starzecki, G. DeAngelis, B. Rubio, J. Styczen, K. Zuber, H. Güven, W. Urban, W. Gast, P. Kleinheinz, S. Lunardi, F. Soramel, A. Facco, C. Signorini, M. Morando, W. Meczynski, A. M. Stefanini, and G. Fortuna, Phys. Lett. B **200**, 419 (1988).

[8] B. G. Carlsson, I. Ragnarsson, R. Bengtsson, E. O. Lieder, R. M. Lieder, and A. A. Pasternak, Phys. Rev. C **78**, 034316 (2008).

[9] M. Müller-Veggian, H. Beuscher, D. R. Haenni, R. M. Lieder, A. Neskakis, and C. Mayer-Böricke, Nucl. Phys. A **344**, 89 (1980).

[10] H. L. Liu and F. R. Xu, Chin. Phys. Lett. **25**, 1621 (2008).

[11] A. F. Mertz, E. A. McCutchan, R. F. Casten, R. J. Casperson, A. Heinz, B. Huber, R. Lüttke, J. Qian, B. Shoraka, J. R. Terry, V. Werner, E. Williams, and R. Winkler, Phys. Rev. C **77**, 014307 (2008).

[12] M. Müller-Veggian, Y. Gono, R. M. Lieder, A. Neskakis, and C. Mayer-Böricke, Nucl. Phys. A **304**, 1 (1978).

[13] N. Yoshikawa, Nucl. Phys. A **243**, 143 (1975).

[14] R. M. Lieder, T. Rzaca-Urban, H. Brands, W. Gast, H. M. Jäger, L. Mihailescu, Z. Marcinkowska, W. Urban, T. Morek, Ch. Droste, P. Szymański, S. Chmel, D. Bazzacco, G. Falconi, R. Menegazzo, S. Lunardi, C. Rossi Alvarez, G. de Angelis, E. Farnea, A. Gadea, D. R. Napoli, Z. Podolyak, Ts. Venkova, and R. Wyss, Eur. Phys. J. A **13**, 297 (2002).

[15] M. Sugawara, Y. Toh, M. Oshima, M. Koizumi, A. Osa, A. Kimura, Y. Hatsukawa, J. Goto, H. Kusakari, T. Morikawa, Y. H. Zhang, X. H. Zhou, Y. X. Guo, and M. L. Liu, Phys. Rev. C **79**, 064321 (2009).

[16] M. G. Procter, D. M. Cullen, C. Scholey, B. Niclasen, P. J. R. Mason, S. V. Rigby, J. A. Dare, A. Dewald, P. T. Greenlees, H. Iwasaki, U. Jakobsson, P. M. Jones, R. Julin, S. Juutinen, S. Ketelhut, M. Leino, N. M. Lumley, O. Möller, M. Nyman, P. Peura, T. Pissulla, A. Puurunen, P. Rahkila, W. Rother, P.

Ruotsalainen, J. Sarén, J. Sorri, and J. Uusitalo, Phys. Rev. C **81**, 054320 (2010).

[17] S. Rajbanshi, A. Bisoi, S. Nag, S. Saha, J. Sethi, T. Trivedi, T. Bhattacharjee, S. Bhattacharyya, S. Chattopadhyay, G. Gangopadhyay, G. Mukherjee, R. Palit, R. Raut, M. Saha Sarkar, A. K. Singh, and A. Goswami, Phys. Rev. C **89**, 014315 (2014).

[18] P. Ring, Prog. Part. Nucl. Phys. **37**, 193 (1996).

[19] D. Vretenar, A. V. Afanasjev, G. A. Lalazissis, and P. Ring, Phys. Rep. **409**, 101 (2005).

[20] J. Meng, H. Toki, S. G. Zhou, S. Q. Zhang, W. H. Long, and L. S. Geng, Prog. Part. Nucl. Phys. **57**, 470 (2006).

[21] J. Meng, *Relativistic Density Functional for Nuclear Structure* (World Scientific, Singapore, 2016).

[22] T. Nikšić, Z. P. Li, D. Vretenar, L. Prochniak, J. Meng, and P. Ring, Phys. Rev. C **79**, 034303 (2009).

[23] Z. P. Li, T. Nikšić, D. Vretenar, J. Meng, G. A. Lalazissis, and P. Ring, Phys. Rev. C **79**, 054301 (2009).

[24] Z. P. Li, T. Nikšić, D. Vretenar, and J. Meng, Phys. Rev. C **80**, 061301(R) (2009).

[25] Z. P. Li, T. Nikšić, D. Vretenar, P. Ring, and J. Meng, Phys. Rev. C **81**, 064321 (2010).

[26] Z. P. Li, J. M. Yao, D. Vretenar, T. Nikšić, H. Chen, and J. Meng, Phys. Rev. C **84**, 054304 (2011).

[27] Z. P. Li, C. Y. Li, J. Xiang, J. M. Yao, and J. Meng, Phys. Lett. B **717**, 470 (2012).

[28] Y. Fu, H. Mei, J. Xiang, Z. P. Li, J. M. Yao, and J. Meng, Phys. Rev. C **87**, 054305 (2013).

[29] K. Q. Lu, Z. X. Li, Z. P. Li, J. M. Yao, and J. Meng, Phys. Rev. C **91**, 027304 (2015).

[30] Z. P. Li, T. Nikšić, and D. Vretenar, J. Phys. G **43**, 024005 (2016).

[31] T. Nikšić, D. Vretenar, and P. Ring, Prog. Part. Nucl. Phys. **66**, 519 (2011).

[32] V. Prassa, T. Nikšić, G. A. Lalazissis, and D. Vretenar, Phys. Rev. C **86**, 024317 (2012).

[33] V. Prassa, T. Nikšić, and D. Vretenar, Phys. Rev. C **88**, 044324 (2013).

[34] J. Xiang, J. M. Yao, Y. Fu, Z. H. Wang, Z. P. Li, and W. H. Long, Phys. Rev. C **93**, 054324 (2016).

[35] L. Próchniak, P. Quentin, D. Samsoen, and J. Libert, Nucl. Phys. A **730**, 59 (2004).

[36] J. Libert, M. Girod, and J.-P. Delaroche, Phys. Rev. C **60**, 054301 (1999).

[37] P. W. Zhao, Z. P. Li, J. M. Yao, and J. Meng, Phys. Rev. C **82**, 054319 (2010).

[38] Y. Tian, Z. Y. Ma, and P. Ring, Phys. Lett. B **676**, 44 (2009).

[39] T. Nikšić, P. Ring, D. Vretenar, Y. Tian, and Z. Y. Ma, Phys. Rev. C **81**, 054318 (2010).

[40] J. Xiang, Z. P. Li, Z. X. Li, J. M. Yao, and J. Meng, Nucl. Phys. A **873**, 1 (2012).

[41] http://www.nndc.bnl.gov/chart/.

[42] T. Klemme, A. Fitzler, A. Dewald, S. Schell, S. Kasemann, R. Kuhn, O. Stuch, H. Tiesler, K. O. Zell, P. von Brentano, D. Bazzacco, F. Brandolini, S. Lunardi, C. M. Petrache, C. Rossi Alvarez, G. De Angelis, P. Petkov, and R. Wyss, Phys. Rev. C **60**, 034301 (1999).

[43] J.-P. Delaroche, M. Girod, J. Libert, H. Goutte, S. Hilaire, S. Péru, N. Pillet, and G. F. Bertsch, Phys. Rev. C **81**, 014303 (2010).

[44] T. Kibédi and R. H. Spear, At. Data Nucl. Data Tables **89**, 77 (2005).